IEEE Access
Multidisciplinary | Rapid Review | Open Access Journal

Received January 29, 2019, accepted February 9, 2019, date of publication February 21, 2019, date of current version March 8, 2019.

Digital Object Identifier 10.1109/ACCESS.2019.2900799

An Extended Kalman Filter for Direct, Real-Time, Phase-Based High Precision Indoor Localization

MELANIE LIPKA, (Student Member, IEEE), ERIK SIPPEL, AND MARTIN VOSSIEK, (Fellow, IEEE)
Institute of Microwaves and Photonics, Friedrich-Alexander-Universität Erlangen–Nürnberg, 91058 Erlangen, Germany
Corresponding author: Melanie Lipka (melanie.lipka@fau.de)

ABSTRACT Radio-based indoor localization is currently a very vibrant scientific research field with many potential use cases. It offers high value for customers, for example, in the fields of robotics, logistics, and automation, or in context-aware IT services. Especially for autonomous systems, dynamic human–machine interaction, or augmented reality applications, precise localization coupled with a high update rate is a key. In this paper, we present a completely novel localization concept whereby received radio signal phase values that are fed into an extended Kalman filter (EKF) without any preprocessing are evaluated. Standard preprocessing steps, such as angle-of-arrival estimation, beamforming, and time-of-flight or time-difference-of-arrival estimations are not required with this approach. The innovative localization concept benefits from the high sensitivity of radio signals' phase to distance changes and the fast and straightforward recursive computation offered by the EKF. It completely forgoes the computational burden of other phase-based high-precision localization techniques, such as synthetic aperture methods. To verify the proposed method, we use an exemplary setup employing a 24 GHz frequency-modulated continuous-wave (CW) single-input multiple-output secondary radar with 250 MHz bandwidth. A high-precision six-axis robotic arm serves as a 3D positioning reference. The test setup emulates a realistic industrial indoor environment with significant multipath reflections. Despite the challenging conditions and the rather low bandwidth, the results show an outstanding localization 3D RMSE of around 1.7 cm. The proposed method can easily be applied to nearly any type of radio signal with CW carrier and is an attractive alternative to common multilateration and multiangulation localization approaches. We think it is a quantum leap in wireless locating, as it has the potential for precise, simple, and low-cost wireless localization even with standard narrowband communication signals.

INDEX TERMS FMCW, radar, localization, extended Kalman filter, near field, indoor.

I. INTRODUCTION

Indoor localization has growing fields of applications, especially if GPS is not available. Microwave radar is a reasonable candidate for a whole range of wireless local positioning tasks, for example, industrial applications, tracking tools or goods, autonomous storage robots, and many more. Depending on the speeds involved and health and safety regulations, these applications may require very precise localization and high update rates, while the complexity, and therefore the cost of the necessary infrastructure, needs to be minimized.

Conventional techniques for wireless positioning are angle-of-arrival (AOA), round-trip-time-of-flight (RTOF), time-difference-of-arrival (TDOA) or received-signal-strength (RSS), see [1]–[3]. Depending on the indoor use case, these methods have different challenges and drawbacks.

RSS based localization relies on signal strength received from several landmarks, like radio frequency identification tags [4] or wifi hotspots [5]. Especially under noisy conditions, like in industrial settings, the technique is too sensitive to changes in the environment and requires continuous surveillance of the surroundings, while being insensitive to location changes. Although inertial sensors may improve localization accuracy [6], generating an adequate map of wifi fingerprints, for example, is time-consuming. Sophisticated mapping methods may reduce the effort required, as well as the number of labeled fingerprints [7].

The associate editor coordinating the review of this manuscript and approving it for publication was Mehmet Alper Uslu.

Another approach would be transit-time-based methods, requiring accurate synchronization, see [8], and [9], or coherent transponders. Applications using this basic concept of multilateral are manifold. Examples are self-localization using a grid of known landmarks with fixed positions [10] or the reverse scenario locating a tag attached to a vehicle [11]. As the bandwidth determines the range accuracy, ultra wideband (UWB) systems are particularly suitable for precise multiangulation tasks [12]. As non-synchronized, non-coherent beacons should be used, where possible, TOF- and RTOF-based methods are effectively ruled out.

In contrast to these techniques, the proposed solution relies solely on the phase differences between the signals received at distributed antennas. The conventional approach would be to determine the AOA with a beamformer, e.g., Delay and Sum or MUSIC. Specifically, the angle for every fixed station is calculated first, then the location is determined using the combined information from multiple base stations [13]. In landmark-based scenarios, a mobile station measures the angle to multiple fixed transponders [14] and computes its pose and position. In order to determine the AOA, the transmitter is assumed to be located in the far field of the base station. To achieve high precision for close ranges, the curvature of the wave front would have to be considered [15]. This would require information about the distance to the transmitter.

Furthermore, angulation and lateration may be combined, as shown in [16]. The most significant strength of this concept is the minimal infrastructure needed for localization. Nevertheless, it suffers from the drawbacks of AOA and TOF already mentioned above and is therefore not employable for unsynchronized systems.

Other approaches for high precision localization using a moderate bandwidth, are synthetic aperture concepts, shown in [17] and [18]. But the high precision achieved with these methods comes at the expense of high computational effort.

In the light of these issues and challenges, we propose an approach that evaluates the measured phase differences directly using a computationally efficient Extended Kalman Filter (EKF). The approach resolves occurring ambiguities in a recursive manner and can take advantage of the high phase sensitivity at elevated carrier frequencies. It also deals with the problem of unknown phases for incoherent systems and proves itself suitable for various infrastructures, while requiring low computational effort.

The sections in this paper are organized as follows. First, the general signal model and assumptions for the filter are presented. Then, the proposed EKF is described and the compositions of the individual matrices are specified. Finally, the algorithm is verified using a 24GHz secondary frequency modulated continuous wave (FMCW) radar in an indoor near field localization scenario, and the results are presented.

II. SYSTEM MODEL

In order to extract the location from a wireless positioning system, a relation between the position of an object or transmitter and the input data is required. In this work, an object emitting the signal

$$s_{\mathrm{TX,RF}}(t) = s_{\mathrm{TX,BB}}(t)\mathrm{e}^{\mathrm{j}\omega_0 t+\phi_0} \tag{1}$$

shall be located, where $\omega_0 = 2\pi f_0$ denotes the carrier frequency, ϕ_0 represents an unknown phase offset, and $s_{\mathrm{TX,BB}}(t)$ denotes a slowly varying base band signal. Here, no assumptions about the signal origin are made and hence, the signal $s_{\mathrm{TX,RF}}(t)$ may be reflected from the object or be emitted on purpose by a wireless transmitter. Furthermore, no special signal form is assumed and therefore any arbitrary transmitter, like a communication device, that emits a signal can be localized. For this purpose, M base stations at fixed locations, each equipped with an arbitrary number I_m of coherently receiving antennas are available. Hence, the signal

$$s_{i_m}(t) = a_{i_m} \cdot s_{\mathrm{TX,BB}}(t-\tau_{i_m})\mathrm{e}^{j(\omega_0(t-\tau_{i_m})+\phi_0+\phi_m)} \tag{2}$$

is received at each antenna. Here a_{i_m} represents an attenuation factor, ϕ_m denotes the unknown phase offset of the m-th station and the transmitted signal requires $\tau_{i_m} = \frac{r_{i_m}}{c_0}$ to travel the distance

$$r_{i_m} = \sqrt{(x_{i_m}-p_x)^2 + (y_{i_m}-p_y)^2 + (z_{i_m}-p_z)^2} \tag{3}$$

from the object at $[p_x, p_y, p_z]$ to receive antenna i_m at $[x_{i_m}, y_{i_m}, z_{i_m}]$. In order to locate the object, the phase difference between each pair of coherently receiving antennas $i_m \neq j_m$, (Fig. 1), is evaluated by correlating the received signals $s_{i_m}(t)$ and $s_{j_m}(t)$ of the i-th and j-th antenna, respectively, at the m-th station

$$\begin{aligned}\int & s^*_{i_m}(t)s_{j_m}(t)\mathrm{d}t \\ &= \int a_{i_m}s^*_{\mathrm{TX,BB}}(t-\tau_{i_m})\mathrm{e}^{-\mathrm{j}(\omega_0(t-\tau_{i_m})+\phi_0+\phi_m)} \cdot \\ &\quad \cdot a_{j_m}s_{\mathrm{TX,BB}}(t-\tau_{j_m})\mathrm{e}^{\mathrm{j}(\omega_0(t-\tau_{j_m})+\phi_0+\phi_m)}\mathrm{d}t \\ &= \int a \cdot s^*_{\mathrm{TX,BB}}(t-\tau_{i_m})s_{\mathrm{TX,BB}}(t-\tau_{j_m})\mathrm{e}^{\mathrm{j}\omega_0(\tau_{i_m}-\tau_{j_m})}\mathrm{d}t\end{aligned}$$

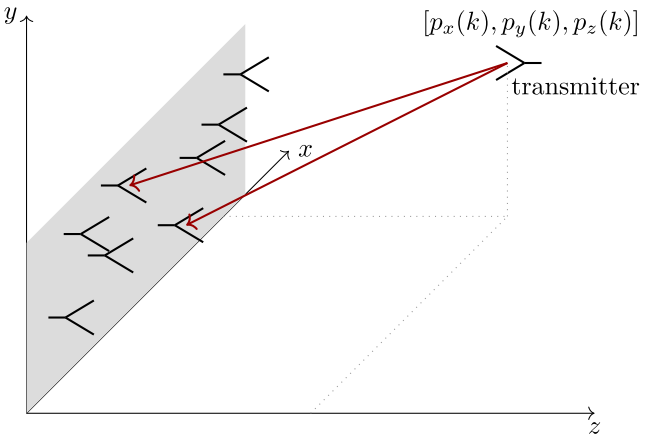

FIGURE 1. Configuration of one base station with 8 coherent receive channels and a transmitter located at $[p_x(k), p_y(k), p_z(k)]$.

$$\approx a \cdot \int \left| s_{\mathrm{TX,BB}}(t-\tau_{i_m}) \right|^2 \mathrm{e}^{\mathrm{j}\omega_0(\tau_{i_m}-\tau_{j_m})} \mathrm{d}t$$
$$= a \cdot \mathrm{e}^{\mathrm{j}\omega_0(\tau_{i_m}-\tau_{j_m})} \int \left| s_{\mathrm{TX,BB}}(t-\tau_{i_m}) \right|^2 \mathrm{d}t, \quad (4)$$

where $a = a_{i_m} \cdot a_{j_m}$, and $s_{\mathrm{TX,BB}}(t-\tau_{i_m}) \approx s_{\mathrm{TX,BB}}(t-\tau_{j_m})$ holds, as the modulation signal $s_{\mathrm{TX,BB}}(t)$, is considered slowly varying. Hence, a position-dependent phase difference between each antenna pair is originated (this is well suited for localization). Generally speaking, the phase difference can be evaluated in different ways, especially if specific types of radar systems, such as FMCW or OFDM, are used. The general dependency

$$\Delta\varphi_{m,i-j} = \omega_0(\tau_{i_m} - \tau_{j_m}) \quad (5)$$

of the phase difference between the coherently receiving i_m-th and j_m-th antenna at the m-th receive station holds, nonetheless. The difference may be ambiguous depending on the antenna positions and is mapped to the interval $[-\pi, \pi]$ as

$$\Delta\varphi_{m,ij} = \begin{cases} \mathrm{mod}_{2\pi}(\Delta\varphi_{m,i-j}), & \text{for } \mathrm{mod}_{2\pi}(\varphi_{m,i-j}) < \pi, \\ \mathrm{mod}_{2\pi}(\Delta\varphi_{m,i-j}) - 2\pi, & \text{for } \mathrm{mod}_{2\pi}(\varphi_{m,i-j}) > \pi. \end{cases} \quad (6)$$

We assume, for the sake of simplicity, that all antenna elements have the same directivity pattern and the phase center is independent within the used bandwidth, and that phase shifts caused by length imbalances and other hardware impairments have been calibrated. Furthermore, the position of each individual antenna is known. Kalman filters have proven themselves robust against nonidealities, see [19].

III. EXTENDED KALMAN FILTER

Although the phase difference is only known in the interval $[-\pi, \pi]$, ambiguity is handled by using a recursive filter locating the transmitter in the surroundings of its location, that is predicted by preceding measurements. A well-suited algorithm for this task is the proposed EKF, see [19]–[21], which is described in the following sections. Although it is computationally very efficient, it is still just one of many possible ways of implementing the basic idea of recursively locating an incoherent transmitter based on the evaluation of phase differences for coherent receive channels.

A Kalman filter typically consists of two steps, the state transition (prediction) and its correction (update). In an optimal case, the function relating the last state x_{k-1} with the predicted current state x_k should be a linear function with added Gaussian noise

$$x_k = F x_{k-1} + n_k, \quad (7)$$

where x_k is the state at sample point k, F the transition matrix, and n_k is a random vector with Gaussian distributed entries described by the covariance matrix Q.

The same conditions apply for the function relating measurement and state, and for optimality it must be linear in its arguments [19]. This function is given by

$$z_k = H_k x_k + w_k, \quad (8)$$

where z_k is the vector containing the measurements, H_k denotes the matrix for the conversion from the measurement to the state domain, and w_k is a vector with Gaussian distributed entries described by the covariance matrix R.

The corresponding equations for the proposed Kalman filter are derived in the next section. First, the state vector is defined, then a quick overview for one possible prediction step is given. Finally, the general equations for the proposed novel update concept are shown and the compositions of the individual matrices are described in-depth.

A. STATE VECTOR

First, the state vector for the localization problem is defined as

$$x_k = \left[p_x(k), p_y(k), p_z(k), v_x(k), v_y(k), v_z(k)\right]^{\mathrm{T}} \quad (9)$$

at sampling point k with $p_x(k), p_y(k), p_z(k)$ as the Cartesian coordinates of the transmitter and their corresponding speed components $v_x(k), v_y(k), v_z(k)$. Kalman filters generally assume Markov processes, i.e., each state x_k is fully described and stochastically dependent on its preceding state x_{k-1}, as in (7). Unfortunately, the Markov assumption does not hold for radar systems, as the environment affects the motion statistics. Nevertheless, Kalman filters have proven themselves to be very robust to such violations [19].

B. PREDICTION

In order to predict the location, we assume that the transmitter moves with almost constant velocity [22]. Accelerations are handled in the process noise covariance. Therefore, the location can be predicted by applying the equation of motion, resulting in the linear state transition

$$x_{k|k-1} = F \cdot x_{k-1|k-1} = \begin{bmatrix} 1 & 0 & 0 & \Delta T & 0 & 0 \\ 0 & 1 & 0 & 0 & \Delta T & 0 \\ 0 & 0 & 1 & 0 & 0 & \Delta T \\ 0 & 0 & 0 & 1 & 0 & 0 \\ 0 & 0 & 0 & 0 & 1 & 0 \\ 0 & 0 & 0 & 0 & 0 & 1 \end{bmatrix} \cdot x_{k-1|k-1}, \quad (10)$$

where $x_{k|k-1} = \left[p'_x(k), p'_y(k), p'_z(k), v'_x(k), v'_y(k), v'_z(k)\right]^{\mathrm{T}}$ denotes the predicted location, ΔT the time between two adjacent sampling points, and F the state transition matrix.

The expected covariance matrix $P_{k|k-1}$ is calculated from the covariance $P_{k-1|k-1}$ at sampling point $k-1$ and the process noise covariance matrix Q [19]–[21] as

$$P_{k|k-1} = F \cdot P_{k-1|k-1} \cdot F^{\mathrm{T}} + Q. \quad (11)$$

The state obtained in this step is an assumption for the likely new position. Since no sampled data have been considered so far, the uncertainty due to increasing covariance

matrix entries rises. The process noise covariance matrix Q is derived from the possible misjudgment of position and velocity, mainly due to the acceleration with variance σ_a^2, which is assumed constant between two sampling points and has been neglected in the prediction step. Incorporating it into the variance results in the covariance matrix

$$Q = \sigma_a^2 \cdot \begin{bmatrix} \frac{\Delta T^4}{4} & 0 & 0 & \frac{\Delta T^3}{2} & 0 & 0 \\ 0 & \frac{\Delta T^4}{4} & 0 & 0 & \frac{\Delta T^3}{2} & 0 \\ 0 & 0 & \frac{\Delta T^4}{4} & 0 & 0 & \frac{\Delta T^3}{2} \\ \frac{\Delta T^3}{2} & 0 & 0 & \Delta T^2 & 0 & 0 \\ 0 & \frac{\Delta T^3}{2} & 0 & 0 & \Delta T^2 & 0 \\ 0 & 0 & \frac{\Delta T^3}{2} & 0 & 0 & \Delta T^2 \end{bmatrix}, \tag{12}$$

which reflects the uncertainty about how position and velocity may have altered within the elapsed time ΔT because the acceleration has not been modeled. The variance σ_a^2 should be chosen appropriately to reflect the actual acceleration and may differ significantly in different scenarios, like tracking vehicles or persons, or the rapid movements of human limbs. If the variance is chosen too low, strong accelerations like turnarounds can't be tracked properly. On the other hand, if the variance is chosen too high, the uncertainty increases more in the prediction step and the EKF puts more trust in the measurements. In the limiting case, the filter would only trust the measurements and completely loose the benefits of exploiting motion statistics.

C. UPDATE

The relation between state (position, velocity) and sampled data (phase differences) is a nonlinear function that must be linearized, hence the EKF equations are applicable.

The input data is merged with the prediction in this step. The Kalman gain

$$K_k = P_{k|k-1} H_k^T (H_k P_{k|k-1} H_k^T + R)^{-1} \tag{13}$$

is calculated for this purpose, with H_k denoting the Jacobian matrix obtained from the output transition function $h(x_{k|k-1})$ and R the measurement noise covariance matrix. The phase variance can be determined empirically and adjusted for a proper weighting of the measurement. Small matrix entry values in R imply that the EKF puts more trust in the measurements, while small matrix entries in Q means more trust for the prediction. Hence, the relation between R and Q must be chosen properly for best accuracy. The Kalman Gain is then used to update the state and its covariance matrix using the standard EKF formulas [19]–[21] as

$$x_{k|k} = x_{k|k-1} + K_k(\text{inno}_k(x_{k|k-1})), \tag{14}$$

$$P_{k|k} = (I_6 - K_k H_k) P_{k|k-1} \tag{15}$$

where $x_{k|k}$, and $P_{k|k}$ respectively denote the updated position and covariance, I_6 is a 6×6 identity matrix, and z_k contains the sampled phase information obeying equation (5). The innovation $\text{inno}_k(x_{k|k-1})$ represents the difference between the actual data and the values expected due to prediction. Then, the Kalman gain balances the data and prediction uncertainties, and inverts the measurement model in order to update the state in (14). The smaller covariance after applying (15) reflects the lower uncertainties. In the next section, we give a detailed description of how the matrices and vectors are composed for the proposed filter.

1) MEASUREMENT VECTOR

The measurement vector consists of the phase differences obtained from the correlation, as in (5). For every radar station m, all phase difference permutations of the I_m antennas are formed

$$\Delta\varphi_m = \begin{bmatrix} \Delta\varphi_{m,12} \\ \vdots \\ \Delta\varphi_{m,ij} \\ \vdots \\ \Delta\varphi_{m,I(I-1)} \end{bmatrix} \tag{16}$$

and combined to the final measurement vector, taking into account all used base stations, to yield

$$z_k = \begin{bmatrix} \Delta\varphi_1 \\ \vdots \\ \Delta\varphi_m \\ \vdots \\ \Delta\varphi_M \end{bmatrix}, \tag{17}$$

which is now a vector containing $M\frac{I(I-1)}{2}$ entries representing all measurement information. If any other sensor, like an inertial measurement unit, is used, the measurement vector can simply be expanded by appending these values.

2) OUTPUT TRANSITION FUNCTION AND MATRIX

The output transition function $h(x_{k+1|k})$ converts the predicted state vector, i.e. the position and velocity, into the measurement domain, i.e. the vector of phase differences. Using (5), a relation for the predicted phase

$$\Delta\varphi'_{m,ij} = \omega_0 \frac{(r_{i_m} - r_{j_m})}{c_0} \tag{18}$$

is formed for every permutation, where c_0 is the speed of light in a vacuum, and r_{i_m}, r_{j_m} are the distances between the transmitter and receiver antennas i_m, j_m for the m-th base station based on the predicted state $x_{k+1|k}$. The corresponding distances can be calculated using (3). The output transition is now composed consistent with (17) by taking the same

antenna combinations to form

$$h(x_{k+1|k}) = \begin{bmatrix} \Delta\varphi'_{1,12} \\ \vdots \\ \Delta\varphi'_{m,ij} \\ \vdots \\ \Delta\varphi'_{M,I(I-1)} \end{bmatrix}, \tag{19}$$

representing the expected measurement values, due to the predicted state. Normally, the innovation is calculated as the difference between the actual and predicted values, which results here in an incorrect update due to the phase ambiguity. Hence, the difference between the phase measurement and the prediction is mapped onto the interval $[-\pi, \pi]$ via a modulo operation as

$$\begin{aligned} &\text{inno}_k(x_{k|k-1}) \\ &= \begin{cases} \text{mod}_{2\pi}(\Delta_k), & \text{for} \quad \text{mod}_{2\pi}(\Delta_k) < \pi, \\ \text{mod}_{2\pi}(\Delta_k) - 2\pi, & \text{for} \quad \text{mod}_{2\pi}(\Delta_k) > \pi, \end{cases} \\ &\text{with } \Delta_k = z_k - h(x_{k|k-1}). \end{aligned} \tag{20}$$

To calculate the Kalman gain (13) and the covariance matrix (15), H_{k+1} must be calculated. For this purpose, the Jacobian matrix of $h(x_{k|k-1})$ for the state vector is formed as

$$H_{k+1} = \begin{bmatrix} \frac{\partial\Delta\varphi'_{1,12}}{\partial p'_x(k)} & \frac{\partial\Delta\varphi'_{1,12}}{\partial p'_y(k)} & \frac{\partial\Delta\varphi'_{1,12}}{\partial p'_{z(k)}} & 0 & 0 & 0 \\ \vdots & \vdots & \vdots & \vdots & \vdots & \vdots \\ \frac{\partial\Delta\varphi'_{1,I(I-1)}}{\partial p'_x(k)} & \frac{\partial\Delta\varphi'_{1,I(I-1)}}{\partial p'_y(k)} & \frac{\partial\Delta\varphi'_{1,I(I-1)}}{\partial p'_z(k)} & 0 & 0 & 0 \\ \vdots & \vdots & \vdots & \vdots & \vdots & \vdots \\ \frac{\partial\Delta\varphi'_{m,ij}}{\partial p'_x(k)} & \frac{\partial\Delta\varphi'_{m,ij}}{\partial p'_y(k)} & \frac{\partial\Delta\varphi'_{m,ij}}{\partial p'_z(k)} & 0 & 0 & 0 \\ \vdots & \vdots & \vdots & \vdots & \vdots & \vdots \\ \frac{\partial\Delta\varphi'_{M,I(I-1)}}{\partial p'_x(k)} & \frac{\partial\Delta\varphi'_{M,I(I-1)}}{\partial p'_y(k)} & \frac{\partial\Delta\varphi_{M,I(I-1)}}{\partial p'_z(k)} & 0 & 0 & 0 \end{bmatrix} \tag{21}$$

with

$$\frac{\partial\Delta\varphi'_{m,ij}}{\partial p'_x(k)} = \frac{\omega_0}{c}\left(\frac{(p'_x(k) - x_i)}{r_i} - \frac{(p'_x(k) - x_j)}{r_j}\right), \tag{22}$$

$$\frac{\partial\Delta\varphi'_{m,ij}}{\partial p'_y(k)} = \frac{\omega_0}{c}\left(\frac{(p'_y(k) - y_i)}{r_i} - \frac{(p'_y(k) - y_j)}{r_j}\right), \tag{23}$$

$$\frac{\partial\Delta\varphi'_{m,ij}}{\partial p'_z(k)} = \frac{\omega_0}{c}\left(\frac{(p'_z(k) - z_i)}{r_i} - \frac{(p'_z(k) - z_j)}{r_j}\right). \tag{24}$$

Since the phase depends only on the location, the deviation for the velocity and therefore the three right-hand columns of the Jacobian are zero. If an additional sensor, like an accelerometer is used, the matrix must be extended by an additional line, incorporating the relationship of the new sensor to the state.

3) MEASUREMENT NOISE COVARIANCE MATRIX

Although we consider individual phase noise terms to be uncorrelated, each absolute phase term is evaluated in several phase differences and hence, the measurement noise becomes correlated, i.e., a non-diagonal matrix covariance matrix arises. We can distinguish four different types of matrix elements deduced from the phase variance σ^2:

- Differences which don't have any phase value in common and are therefore uncorrelated yield

$$\text{Cov}(\varphi_n - \varphi_m, \varphi_o - \varphi_l) = 0, \quad \text{with } n \neq m \neq o \neq l \in [0, ..., I]. \tag{25}$$

- Elements in the main diagonal yield

$$\text{Var}(\varphi_n - \varphi_m) = \text{Var}(\varphi_n) + \text{Var}(\varphi_m) = 2\sigma^2. \tag{26}$$

- Differences which have one phase value φ_n in common yield

$$\text{Cov}(\varphi_n - \varphi_m, \varphi_n - \varphi_l) = \sigma^2. \tag{27}$$

- Differences which have one phase value φ_n in common, but are evaluated with different signs, yield

$$\text{Cov}(\varphi_n - \varphi_m, -\varphi_n + \varphi_l) = -\sigma^2. \tag{28}$$

If the system comprises multiple base stations, their respective phases can be considered independent and uncorrelated and therefore their covariance is zero. Furthermore, it should be mentioned that the phase variance is not necessarily the same for all base stations. Especially if the signal-to-noise ratio at the different stations is expected to differ, due to different ranges, for instance, it may be useful to adapt the variance based on the predicted location.

D. PHASE AMBIGUITY AND SYSTEM INTERVAL

The EKF resolves the phase ambiguity by recursively taking into account the Kalman state. Nevertheless, this is only possible if antenna distances and sampling rates are matched to the real accelerations. Ambiguity occurs, if the hypothetically correct update step yields a phase difference of more than π and hence fails due to the modulo operation in (20). For simplicity but without loss of generality, only one antenna pair is considered in the following. This is sufficient as the worst ambiguity is generated by the antenna pair separated from each other by the greatest distance. Fig. 2 shows exemplar phase-difference patterns for two different inter-antenna distances d_a. Clearly, the largest phase difference change and therefore the worst case concerning ambiguity appears, when the transponder is located in front of the array and shifts

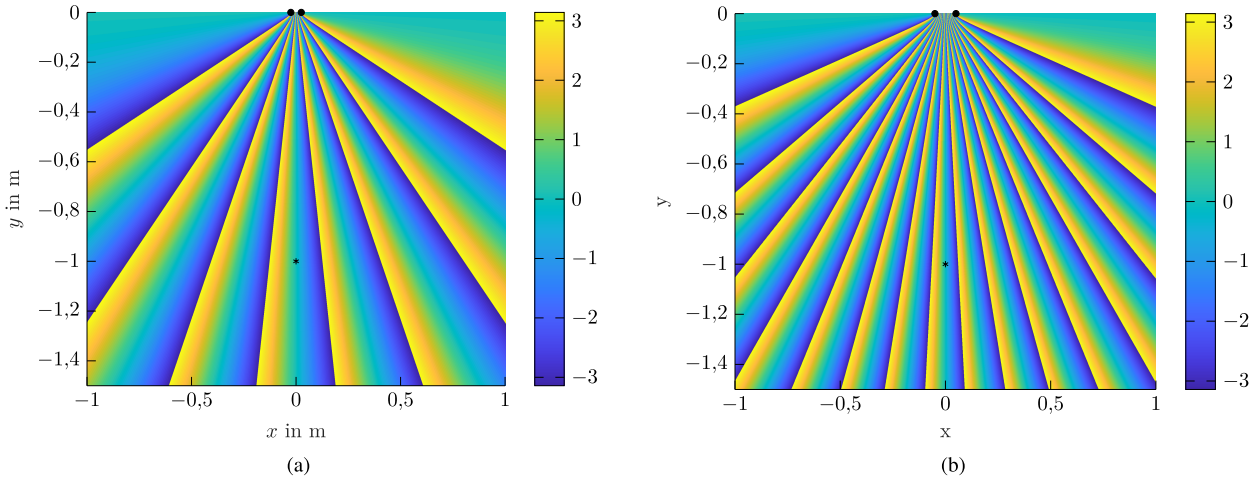

FIGURE 2. Phase difference pattern for a 24GHz transponder (asterisk) and two antenna elements (a) d_a =5 cm (b) d_a =10 cm apart.

parallel to it. Moving the transponder at distance d from $x = -p_x$ to $x = p_x$, yields a phase difference change of

$$\begin{aligned}\Delta(\Delta\varphi_{m,ij}) &= 2\pi \frac{\Delta(r_{i_m} - r_{j_m})}{\lambda_0} \\ &= \frac{2\pi}{\lambda_0} \cdot 2\sqrt{\left(\frac{d_\mathrm{a}}{2} - p_x\right)^2 + d^2}, \end{aligned} \tag{29}$$

where λ_0 denotes the wavelength at carrier frequency and d_a the inter-antenna distance. Hence, a maximum position update of

$$\Delta x = 2p_x = d_\mathrm{a} - \sqrt{\lambda_0^2 - 4d^2} \tag{30}$$

is possible for a transponder-to-array distance of d. Fig. 2 also shows, that the smaller distance between the antennas d, the smaller the unambiguous x-range. The ambiguity impact on localization then depends on the motion model. Assuming a constant velocity model, the maximum acceleration is limited. Unfortunately, the preceding prediction might be corrupted by noise, coupling, multipath, etc. and hence some safety margin should be considered. For a transponder not located in front of the antenna array, i.e. $x \neq 0$, in Fig. 2, a smaller effective inter-antenna distance and a larger unambiguous area emerges. A large antenna array or a close transponder maximizes the sensitivity. In contrast, for a big unambiguous range either the antenna elements must be chosen close to each other or the transponder moves further away from the array.

Unfortunately, given that radial movements from or to the origin cause no change in the phase difference, additional antennas are required for localization.

In summary, ambiguities can be tackled mainly by either arranging the antennas closer to each other or increasing the sampling rate. In addition, an elaborate prediction also contributes to the unambiguousness. Generally, the EKF is very computationally efficient since it consists mainly of additions, differences, multiplications and one matrix inversion. The number of evaluated phase differences defines the matrix dimensions and hence the computational effort is independent of the size of the measurement area. In contrast, other phase-based approaches like beamforming and holography classically search for the transponder on a discrete grid and therefore their computational effort scales with the search area's size and dimension.

E. INTERPRETATION AND ADVANTAGES

The classical localization approach relying only on phase information would be to evaluate the angle-of-arrival using a beamformer or imaging algorithms. Multiple radar base stations are deployed for AOA and some kind of multiangulation or an angle-based EKF [13] may be used for positioning. But this means that beamforming and therefore intricate searching is needed. Imaging techniques, such as interferometry or synthetic aperture radiometry, imply a similar drawback and require far more processing power than the proposed EKF.

The advantages of direct evaluation of the phases for localization and especially for the proposed EKF are outlined in the following section.

One advantage of phase-based localization over techniques computing the angle is that the phases are used directly in the update step. Consequently, a computationally complex maximum search in the beamformers pseudo-spectrum is not required, and every phase is considered separately. This results in a total of $M\frac{I(I-1)}{2}$ values instead of M values for multiangulation. Single erroneous measurements are therefore compensated more easily due to redundancy.

In order to obtain optimal prerequisites for the Kalman filter, the measurement noise should be normally distributed and with known dependency. The noise overlaying the sampled phase values originates from various sources like hardware components or radiation from other devices. Considering the central limit theorem, we can assume that the overall noise is normally distributed [23]. Generally speaking, there are two

different views on phase noise in the literature. It may be considered as an additive term in the phase [24] as

$$s_{\mathrm{n}}(t) = A_{\mathrm{n}}(t)\mathrm{e}^{\mathrm{j}(\theta+\theta_{\mathrm{n}}(t))}, \tag{31}$$

where $s_{\mathrm{n}}(t)$ is the noisy signal, $A_{\mathrm{n}}(t)$ is the noisy amplitude, θ represents the noise free phase, and $\theta_{\mathrm{n}}(t)$ the overlaying Gaussian noise, which may for example originate from phase jitter in PLLs.

The other way would be to consider additive noise to the whole signal as

$$s_{\mathrm{n}}(t) = s(t) + n(t), \tag{32}$$

with $s(t)$ representing the complex noise free signal and $n(t)$ complex Gaussian noise, which may originate from cosmic radiation or other devices. Reference [25] shows that this additive noise causes an approximately Gaussian-shaped probability density function for the phase. In conclusion, the phase noise can be well approximated as normally distributed in both cases.

In contrast, beamformers may suffer from ambiguities depending on the array used. In consequence, a systematic error for designated angle values may occur due to abrupt changes in measured angles.

Another advantage of close-range positioning is that, in contrast to AOA, we do not need to assume a plane wave or compensate the wavefront. This is because all antennas are considered individually, and the curvature is implicitly contained in the relation between state and sampled data.

Furthermore, beamformers require relatively small arrays in order to maintain unambiguousness [26]. For the proposed algorithm, unambiguousness is achieved by elaborate choice of array size and update rate, or if this is not possible, by observing the covariance $P_{k|k}$ over time.

In reverse conclusion, the antenna elements can be chosen further apart, thus increasing the sensitivity of the phase difference to location changes. Thus, coupling between the antennas, and hence systematic errors, are reduced. Additionally, the variety of multipaths at the antennas increases as the distance between them increases. The phase error induced by multipath can be considered increasingly random and thereby independently normally distributed for the antennas.

Finally, the EKF is a computationally efficient algorithm, and especially if phase based, the maximum search in the pseudospectrum for a beamformer is omitted. The less time needed to calculate localization results, the faster the location is updated and, hence, the more suited the system is for safety-critical tasks.

IV. EXPERIMENTAL RESULTS

A. EXPERIMENTAL SETUP

The test setup for algorithm verification is shown in Fig. 3. It consists of three fixed radar stations [27], each equipped with a sparse array of 8 receive antennas [26], originally intended for beamforming, and a smaller mobile transmitter with one transmit channel. The position and tilt of the individual fixed radar stations are determined in-situ before

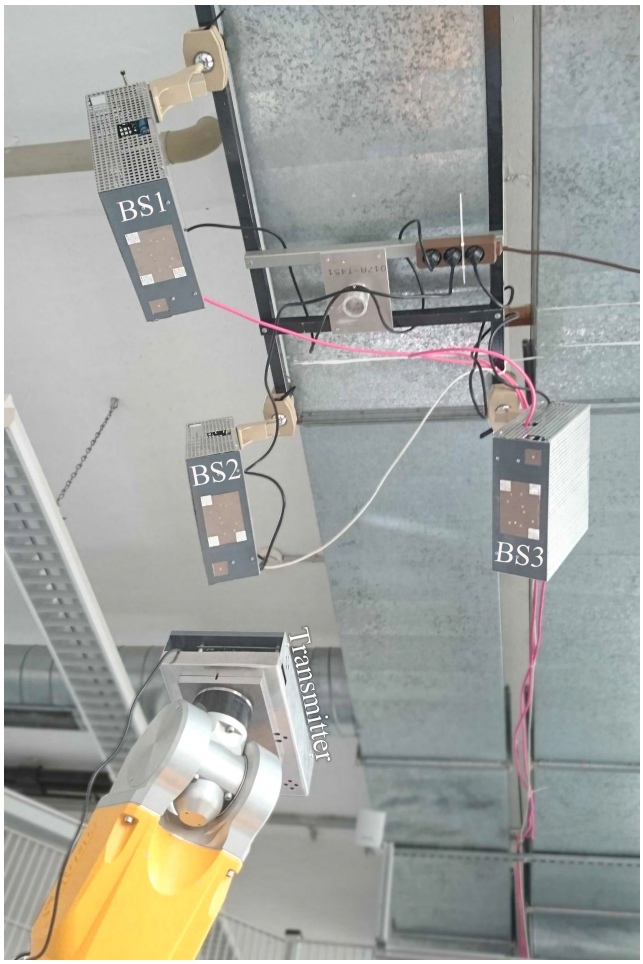

FIGURE 3. Experimental setup featuring three base stations (BS1, BS2, BS3) with two TX and 8 RX channels each, one mobile transmitter with two RX and one TX, and a robotic arm.

measurement. The individual antenna positions can be calculated from station position, tilt and the known antenna array. Each base station consists of eight antennas yielding an array, which is 6.4 cm wide and 3.1 cm high. The system uses the FMCW principle, see [24], with 250 MHz bandwidth and 24 GHz starting frequency, to measure the range and respectively extract the phases received at the spatially distributed antennas. The transmitter is incapable of coherently responding to the FMCW signal, but it is synchronized [8], [9], as it was originally meant for range and angle measurements. As the proposed Kalman filter requires only phase values, it is not necessary to synchronize the transmitter accurately, as long as the signal can be detected in the baseband.

The well-known formula for the low pass filtered FMCW baseband signal

$$S_{\mathrm{BB}} = A_{\mathrm{BB}}\cos(2\pi\mu\tau_{i_m}t + \omega_0\tau_{i_m} + \phi_m) \tag{33}$$

can be employed for the system, where A_{BB} is the amplitude of the baseband signal, μ is the chirp rate, ω_0 is the carrier frequency, and ϕ_m is a characteristic unknown phase term for radar m. The resulting range dependent phase for the

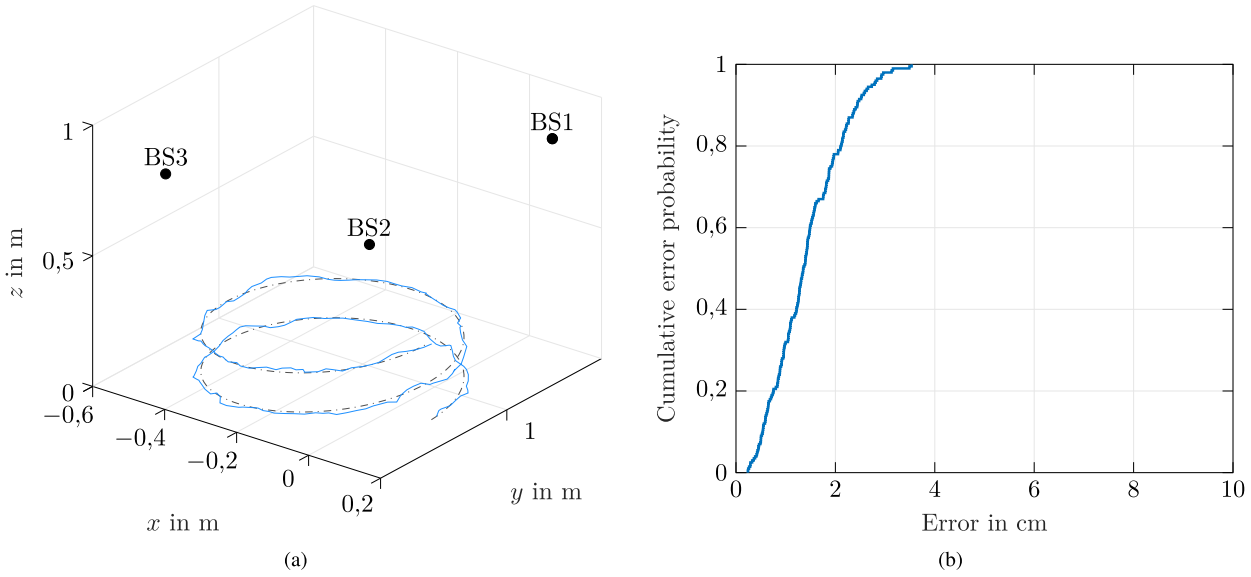

FIGURE 4. (a) 3D view of ideal (grey, dash-dotted) and measured (blue) helix trajectory, where BS1-3 depicts the locations of the base stations. (b) Cumulative RMSE error probability density function for the trajectory using the norm from (35).

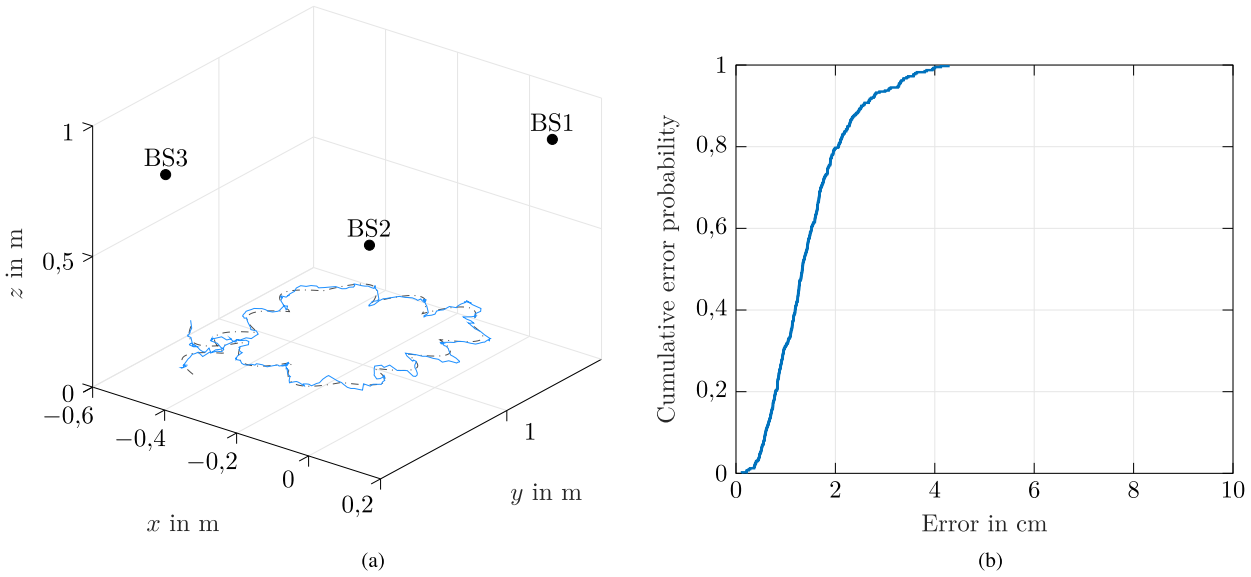

FIGURE 5. (a) 3D view of ideal (grey, dash-dotted) and measured (blue) trajectory with bulges and turns, where BS1-3 depicts the locations of the base stations. (b) Cumulative RMSE error probability density function for the trajectory using the norm from (35).

i-th antenna of the m-th radar is

$$\varphi_i = \omega_0 \tau_{i_m} + \phi_m, \tag{34}$$

in the ideal case. As the receive paths of a real radar suffer from imperfections like different cable lengths for the channels, a phase calibration is carried out in advance. This is crucial for the localization accuracy, since the calculation of the hypothetical phase differences in the update step assumes identical receive channels. Mismatches would cause falsified measurements matching to wrong positions.

A robotic arm is used to move the transmitter in a reproducible manner and simultaneously provide a high precision reference for verifying the localization. The environment is an indoor laboratory with unshielded walls, a metal partition as well as the robotic arm inducing multipath in the scenario.

B. RESULTS

The proposed EKF is now used to compute the location of the transmitter, which is moved by the robotic arm. The known, ideal trajectory is saved for later comparison purposes and algorithmic validation.

First, a helix shaped trajectory as shown in Fig. 4 (a) is driven and evaluated. The ideal trajectory points in this scenario are equally spaced with a distance of about 17 mm.

The cumulative probability of the absolute error is shown in Fig. 4 (b). For the k-th measurement, the error

$$\Delta(k) = \sqrt{\Delta p_x(k)^2 + \Delta p_y(k)^2 + \Delta p_z(k)^2}, \tag{35}$$

is calculated as the 3D distance between the measured and ideal position, see [28], with $\Delta p_x(k)$, $\Delta p_y(k)$, $\Delta p_z(k)$ denoting the difference between the measured and ideal value from the reference.

The RMSE of the overall trajectory is calculated for every Cartesian coordinate as

$$\mathrm{RMSE}_{x,y,z} = \sqrt{\frac{\sum_{l=1}^{L} \Delta p_{x,y,z}(k)^2}{L}}, \tag{36}$$

where x, y, z is the Cartesian coordinate component for which the error is calculated, $\Delta p_{\mathrm{x,y,z}}(k)$ is the difference between the localization result and the corresponding coordinate from the high precision reference at the k-th sampling point, and L is the number of data points. An overall accuracy of $\mathrm{RMSE}_x = 0.99$ cm, $\mathrm{RMSE}_y = 0.59$ cm, and $\mathrm{RMSE}_z = 1.11$ cm has been achieved for the shown track. Differences in the RMSE for the individual directions arise from the extent of the antenna array. The direction with the largest aperture (y-direction) is the most accurate, while the z-direction is the least accurate due to the use of planar arrays facing downwards. Comparing the results to a triangulation-based EKF in the same setup [13], we observe a similar behavior due to the aperture. Our holographic EKF is as such more accurate overall. The accuracy may be further improved by adjusting the array geometry. We should point out though that the array size is limited by the maximum acceleration and the measurement rate.

Another trajectory is shown in Fig. 5 (a), which involves some turns and bulges for a less uniform transmitter motion. In this case, the ideal trajectory points are not equally spaced and are separated by distances of about 5-12 mm. The results are shown in Fig. 5 (b) and can be evaluated for the track as $\mathrm{RMSE}_x = 0.91$ cm, $\mathrm{RMSE}_y = 0.57$ cm, and $\mathrm{RMSE}_z = 1.30$ cm.

V. CONCLUSION

A novel 3D localization algorithm capable of high precision 3D positioning based on phase evaluation is presented in this paper. The Kalman filter implementation offers lower computational effort, in contrast to methods with large search spaces, like conventional beamformers or SAR approaches.

As the algorithm inputs are simply phase difference measurements, the approach is not limited to designated waveforms or large bandwidths. The only limitation is the need for some spatially distributed coherent receive channels. Besides this, any system capable of evaluating distance-dependent phases at coherent receive channels can be used. Thereby the approach enables the use of various transmitter topologies, starting with basic beacons, to non-coherent transmitters and ubiquitous devices, such as cellphones. Conventional systems, like WLAN, mobile communications, Bluetooth, ZigBee and the like, can easily be repurposed for localization without adding designated localization hardware.

REFERENCES

[1] M. Vossiek, L. Wiebking, P. Gulden, J. Wieghardt, C. Hoffmann, and P. Heide, "Wireless local positioning," *IEEE Microw. Mag.*, vol. 4, no. 4, pp. 77–86, Dec. 2003.
[2] P. Gulden, S. Roehr, and M. Christmann, "An overview of wireless local positioning system configurations," in *IEEE MTT-S Int. Microw. Symp. Dig.*, Sep. 2009, pp. 1–4.
[3] K. Pahlavan, X. Li, M. Ylianttila, R. Chana, and M. Latva-Aho, "An overview of wireless indoor geolocation techniques and systems," in *Mobile and Wireless Communications Networks* (Lecture Notes in Computer Science), vol. 1818, C. G. Omidyar, Ed. Berlin, Germany: Springer, 2000, pp. 1–13.
[4] A. Bekkali, H. Sanson, and M. Matsumoto, "Rfid indoor positioning based on probabilistic RFID map and Kalman filtering," in *Proc. 3rd IEEE Int. Conf. Wireless Mobile Comput., Netw. Commun. (WiMob)*, Oct. 2007, p. 21.
[5] A. M. Ladd, K. E. Bekris, A. Rudys, L. E. Kavraki, and D. S. Wallach, "Robotics-based location sensing using wireless Ethernet," in *Proc. 8th Annu. Int. Conf. Mobile Comput. Netw.*, 2002, pp. 227–238.
[6] Z.-A. Deng, Y. Hu, J. Yu, and Z. Na, "Extended Kalman filter for real time indoor localization by fusing WiFi and smartphone inertial sensors," *Micromachines*, vol. 6, no. 4, pp. 523–543, Apr. 2015.
[7] M. Zhou, Y. Tang, W. Nie, L. Xie, and X. Yang, "GrassMA: Graph-based semi-supervised manifold alignment for indoor WLAN localization," *IEEE Sensors J.*, vol. 17, no. 21, pp. 7086–7095, Nov. 2017.
[8] S. Roehr, P. Gulden, and M. Vossiek, "Method for high precision clock synchronization in wireless systems with application to radio navigation," in *Proc. IEEE Radio Wireless Symp.*, Jan. 2007, pp. 551–554.
[9] S. Roehr, P. Gulden, and M. Vossiek, "Novel secondary radar for precise distance and velocity measurement in multipath environments," in *Proc. Eur. Microw. Conf.*, Oct. 2007, pp. 1461–1464 .
[10] J. Pomárico-Franquiz, M. Granados-Cruz, and Y. S. Shmaliy, "Self-localization over RFID tag grid excess channels using extended filtering techniques," *IEEE J. Sel. Topics Signal Process.*, vol. 9, no. 2, pp. 229–238, Mar. 2015.
[11] J. M. Pak, C. K. Ahn, Y. S. Shmaliy, and M. T. Lim, "Improving reliability of particle filter-based localization in wireless sensor networks via hybrid particle/FIR filtering," *IEEE Trans. Ind. Informat.*, vol. 11, no. 5, pp. 1089–1098, Oct. 2015.
[12] Y. Xu, Y. S. Shmaliy, C. K. Ahn, G. Tian, and X. Chen, "Robust and accurate uwb-based indoor robot localisation using integrated ekf/efir filtering," *IET Radar, Sonar Navigat.*, vol. 12, no. 7, pp. 750–756, Jul. 2018.
[13] M. Lipka *et al.*, "Wireless 3D localization concept for industrial automation based on a bearings only extended Kalman filter," in *Proc. Asia–Pacific Microw. Conf. (APMC)*, Kyoto, Japan, Nov. 2018, pp. 821–823.
[14] M. Granados-Cruz, J. Pomárico-Franquiz, Y. S. Shmaliy, and L. J. Morales-Mendoza, "Triangulation-based indoor robot localization using extended FIR/Kalman filtering," in *Proc. 11th Int. Conf. Elect. Eng., Comput. Sci. Autom. Control (CCE)*, Campeche, Mexico, Sep./Oct. 2014, pp. 1–5. [Online]. Available: http://ieeexplore.ieee.org/servlet/opac?punumber=6961334
[15] A. L. Swindlehurst and T. Kailath, "Passive direction-of-arrival and range estimation for near-field sources," in *Proc. 4th Annu. ASSP Workshop Spectr. Estimation Modeling*, Aug. 1988, pp. 123–128.
[16] Y. Dobrev, P. Gulden, and M. Vossiek, "An indoor positioning system based on wireless range and angle measurements assisted by multi-modal sensor fusion for service robot applications," *IEEE Access*, vol. 6, pp. 69036–69052, 2018.
[17] G. Li and M. Vossiek, "A multilateral synthetic aperture wireless positioning approach to precise 3D localization of a robot tool center point," in *Proc. IEEE Top. Conf. Wireless Sensors Sensor Netw. (WiSNet)*, Jan. 2011, pp. 37–40.
[18] R. Miesen, F. Kirsch, and M. Vossiek, "UHF RFID localization based on synthetic apertures," *IEEE Trans. Autom. Sci. Eng.*, vol. 10, no. 3, pp. 807–815, Jul. 2013.
[19] S. Thrun, W. Burgard, and D. Fox, *Probabilistic Robotics*. Cambridge, MA, USA: MIT Press, 2005.
[20] Y. Bar-Shalom, X. R. Li, and T. Kirubarajan, *Estimation with Applications to Tracking and Navigation: Theory Algorithms and Software*, 1st ed. New York, NY, USA: Wiley, 2001.

[21] J. Wendel, *Integrierte Navigationssysteme*. Munich, Germany: De Gruyter Oldenbourg, 2007.
[22] R. G. Brown and P. Y. C. Hwang, *Introduction to Random Signals and Applied Kalman Filtering with Matlab Exercises and Solutions*, 4th ed. Hoboken, NJ, USA: Wiley, 2012.
[23] T. M. Cover and J. A. Thomas, *Elements of Information Theory* (Telecommunications and Signal Processing). Hoboken, NJ, USA: Wiley, 2006.
[24] G. M. Brooker, "Understanding millimetre wave FMCW radars," in *Proc. 1st Int. Conf. Sens. Technol.*, Nov. 2005, pp. 152–157.
[25] J. C. Chang, "The response of hard-limiting bandpass limiters to PM signals," *IEEE Trans. Aerosp. Electron. Syst.*, vol. AES-6, no. 3, pp. 398–400, May 1970.
[26] T. Pavlenko, C. Reustle, Y. Dobrev, M. Gottinger, L. Jassoume, and M. Vossiek, "Design and optimization of sparse planar antenna arrays for wireless 3-D local positioning systems," *IEEE Trans. Antennas Propag.*, vol. 65, no. 12, pp. 7288–7297, Dec. 2017.
[27] Y. Dobrev, M. Vossiek, and D. Shmakov, "A bilateral 24 ghz wireless positioning system for 3D real-time localization of people and mobile robots," in *IEEE MTT-S Int. Microw. Symp. Dig.*, Apr. 2015, pp. 1–4.
[28] Subcommittee for Base Cartographic Data. (1998). *Geospatial Positioning Accuracy Standards Part 3: National Standard for Spatial Data Accuracy*. [Online]. Available: https://www.fgdc.gov/standards/projects/FGDC-standards-projects/accuracy/part3/chapter3

MELANIE LIPKA (S'18) was born in Altdorf, Germany, in 1990. She received the M.Sc. degree in electronic engineering from Friedrich-Alexander-Universität Erlangen–Nürnberg (FAU), Erlangen, Germany, in 2014, where she is currently pursuing the Ph.D. degree with the Institute of Microwaves and Photonics. In 2015, she joined the Institute of Microwaves and Photonics, FAU. Her current research interests include radar for close range applications, indoor positioning, Kalman filter for localization, and signal processing.

ERIK SIPPEL was born in Fürth, Germany, in 1991. He received the M.Sc. degree in electronic engineering from the Friedrich-Alexander-Universität Erlangen–Nürnberg (FAU), Erlangen, Germany, in 2015, where he is currently pursuing the Ph.D. degree.

In 2016, he joined the Institute of Microwaves and Photonics, FAU. His current research interest includes indoor localization, especially radar for near-field localization, data transmission, and analog-to-digital conversion.

MARTIN VOSSIEK (M'96–SM'05–F'16) received the Ph.D. degree from Ruhr University Bochum, Bochum, Germany, in 1996. In 1996, he joined Siemens Corporate Technology, Munich, Germany, where he was the Head of the Microwave Systems Group, from 2000 to 2003. Since 2003, he has been a Full Professor with Clausthal University, Clausthal-Zellerfeld, Germany. Since 2011, he has been the Chair of the Institute of Microwaves and Photonics (LHFT), Friedrich-Alexander University Erlangen–Nürnberg (FAU), Germany. With over 40 researchers, the LHFT is a world-class center for the Microwave and Radar Research and Scholarship. He has authored or co-authored more than 200 papers. His research has led to over 90 granted patents. His current research interests include radar, transponder, RF identification, communication, and locating systems. He has been a member of organizing committees and technical program committees for many international conferences. He is a member of the German IEEE Microwave Theory and Techniques (MTT)/Antennas and Propagation Chapter Executive Board. He was a recipient of several international awards. For example, recently, he was awarded with the prestigious 2019 Microwave Application Award of the IEEE Microwave Theory and Techniques Society (MTT-S) for Pioneering Research in Wireless Local Positioning Systems and for Fostering the Translating of these Innovations into Successful Business in Industrial Automation and Logistics. He was the founding Chair of the MTT IEEE Technical Coordinating Subcommittee MTT-27 Wireless-Enabled Automotive and Vehicular Application, and he is also a member of the Microwave Systems Subcommittee MTT-16. He has served on the review boards of numerous technical journals. Since 2013, he has been an Associate Editor of the IEEE TRANSACTIONS ON MICROWAVE THEORY AND TECHNIQUES.